01,05,08,18

Features of temperature behavior of ESR spectra of Cr^{3+} ions in 3D Dirac semimetal Cd_3As_2

© Yu.V. Goryunov[1], A.N. Nateprov[2]

[1] Zavoisky Physical-Technical Institute, FRC Kazan Scientific Center of RAS, Kazan, Russia
[2] Institute of Applied Physics of Chisinau State University, Chisinau, MD-2028, Moldova,

E-mail: gorjunov@kfti.knc.ru

Received October 27, 2024
Revised November 18, 2024
Accepted November 22, 2024

The temperature behavior of chromium impurity in the Dirac semimetal α-Cd_3As_2 was studied using the electron spin resonance (ESR) method on the Cr^{3+} ion. Small intensity of the ESR spectra on the Cr^{3+} ions definitely points that the main valence state of chromium, as well as other impurities, in this material is the Cr^{2+} state. Some of these ions turn into the valence state of Cr^{3+}. Cr^{3+} ions located in tetrahedral vacancies turn into the anti-ferromagnetic phase at the temperatures above 127 K. The transition is accompanied by a sharp narrowing of the ESR spectrum and a collapse of its hyperfine structure. At the temperatures below 50 K, the remaining magnetic ions located in the positions of cadmium ions turn into the ferromagnetic phase, the appearance of which is indicated by a sharp broadening of the exchange-narrowed resonance line and its strong shift to low resonance fields. The observed inversion of the shape of the exchange-narrowed line of the hyperfine structure of the spectrum requires more detailed study.

Keywords: magnetic resonance, topologic materials, magnetic impurities.

DOI: 10.61011/PSS.2024.11.60082.281

1. Introduction

The possibility of doping of topological Dirac semimetals with both rare earth and iron group ions makes them attractive from the point of view of magnetism, since the interaction of two electronic subsystems (localized and itinerant electrons) [1,2] results in a number of interesting features [3–6]. For this reason a multitude of new physical effects and behavioral features are expected [7] and observed [8–15] for chromium dopant in a 3D Dirac topological semimetal Cd_3As_2. The anisotropy interactions can also be caused by the presence of anisotropy of the orbital magnetic moments of the impurity magnetic ion itself in addition to the fact that to the Ruderman-Kittel-Kasui-Yoshida interaction (RKKY interaction) between impurity magnetic moments in 3D Dirac semimetals is organically inherent by anisotropy because of the hybridization of wave functions (orbitals) localized on impurity electrons with wave functions (orbitals) of the itinerant electrons [8]. .

The situation is relatively simple in the case of doping with ions of transition d-metals (Fe and Mn), which, having the $3d^5$ configuration, are in a purely spin S-state with the total orbital moment of their electrons equal to zero [2], but everything becomes more complicated in case of doping of cadmium arsenide with chromium. Firstly, we can expect an electron spin resonance (ESR) in α-Cd_3As_2 on chromium ions Cr^{2+}, Cr^{3+}, Cr^{4+} based on the presence of magnetic moments in doping chromium ions [16–19]. Secondly, the chromium ion Cr^{2+} has $3d^4$ configuration with $S = 2$, $L = 2$, and its valence state fully corresponds to the substituted ion Cd^{2+}, as, for example, in the case of ESR in fluorite, CaF_2 [18] and $CdGa_2S_4$ [19]. It is obvious that this ion is the main dopant when Cd_3As_2 is doped with chromium. However, the observation of ESR on this Cr^{2+} ion in the frequency X-band is complicated by the strong splitting of the energy levels of Cr^{2+} ion in the crystal field [19], which is larger than the quantum of the radio frequency field, as well as strong spin-phonon coupling, leading to a strong broadening of the ESR lines on Cr^{2+} ion [20]. Thirdly, although the chromium ion Cr^{4+} has $3d^2$ configuration with spin $S = 1$, however, the formation of Cr^{4+} ion in this system is unlikely, as well as its detection in the ESR measurements of the frequency X-band. Thus, only ESR on Cr^{3+} ions should be considered in the case of ESR measurements at frequencies in the X-band. This is the purpose of the present experiment, part of which is described in our previous article in Ref. [21], devoted to the detection of magnetic anisotropy caused by chromium impurity in the paramagnetic state.

The features of the temperature behavior of ESR in chromium-doped cadmium arsenide are narrated in this paper. It is worth reminding that Cr^{3+} ion in $3d^3$ configuration has a spin $S = 3/2$ and an orbital angular momentum $L = 3$, which makes a significant contribution to the magnetic moment of the ion, i. e. the magnetic state of the ion is not purely spin. Hence, the impact of the orbital degree of freedom and hybridization of various valence states of chromium ions with the wave functions of the

free electrons of the matrix Cd_3As_2 on the properties of the material is obvious. An even greater „intrigue“ is created by the fact that the chromium ion Cr^{2+}, which is not observed in the X-band, is also the Jahn-Teller ion [22–25], as a result of which vibronic interactions involving lattice vibrations caused by a change of the configuration of magnetic ion bonds may occur in the system of magnetic impurities. It is expected that, the exchange pairs $Cr^{2+}-Cr^{3+}$ can be formed here in case of chromium doping as in a number of other systems [26]. The formation of magnetic polarons is indicated in Ref. [9] and a negative magnetoresistance is observed under certain conditions along with positive magnetoresistance inherent in a pure material. Observations of features characteristic of both the weak localization and anti-localization modes in the field dependences of the magnetoresistance of chromium-doped samples are related to these issues [13,26–28].

Turning to the experimental part, we would like to emphasize once again that we have learned from our previous studies that the main impurities in α-Cd_3As_2 are divalent dopants that do not supply donor electrons to the conduction band. These electrons occur as a result of the ionization of divalent dopants. At the same time, the electron density from s-electrons is not observed in the cadmium ion substitution position. However, there is an electron density from conduction s-electrons in the same tetrahedral interstitial positions (vacancies). And this imposes certain restrictions on the formation of a hyperfine structure of the ESR spectrum of chromium ions.

2. Experiment

The experimental results discussed in this paper were obtained in one experiment, part of which, related to the anisotropy of the paramagnetic state, is described in Ref. [21]. It should be emphasized here that the study deals with the anisotropy of the paramagnetic state of doping chromium ions, but the matrix Cd_3As_2, which contains paramagnetic ions, is diamagnetic. It is worth reminding that ingots of Cd_3As_2 doped with 0.45 at.% Cr were synthesized at 1023 K by direct interaction of the components: Cd (purity 99.999%), As (99.9999%) and Cr (99.99%) in glass graphite crucibles placed in vacuum sealed quartz ampoules. The crystal structure and stoichiometry were confirmed by energy-dispersive X-ray analysis (EDX) and powder X-ray diffraction (PXRD) and repeat the results presented in our previous papers [14,15]. The ESR measurements were performed in a flow-through helium cryostat in the temperature range of 10−310 K using a standard Bruker BER418 modulation ESR spectrometer operating in the X-band (9.3 GHz). The samples were powders suspended in paraffin and oriented in a strong magnetic field with a particle size of about 4 μm. The orientation corresponded to the magnetic field perpendicular to the ampoule axis and the minimum line width in its angular dependence. The powder sample acquired a certain crystalline texture after exposure to a strong magnetic field at high temperature and solidification of the paraffin as follows from Ref. [21]. Since the axes a and b are equivalent in this structure, it is obvious that the powder particles were oriented in such a way that the axis c was positioned along the magnetic field and later, when the temperature dependence was removed, it was positioned in this way.

3. Results and discussion

3.1. Crystal structure

The PXRD data confirm the identity of the synthesized pure and doped compounds of the low-temperature tetragonal modification of α-Cd_3As_2 [29] with the spatial symmetry group $I4_1cd$ and the lattice parameters $a = b = 12.653$ Å, $c = 25.456$ Å. The crystal lattice parameters of pure α-Cd_3As_2 obtained by the same method were $a = b = 12.6539$ Å, $c = 25.4586$ Å. Each cm^3 of α-Cd_3As_2 contains $2.564 \cdot 10^{20}$ of crystal cells. Each cell contains 160 atoms, in particular 96 ions Cd^{2+} and 64 ions As^{3-}, located in the stoichiometric positions of 16 mutually ordered fragments of antifluorite structures [30]. Moreover, tetrahedral vacancies of a crystal cell can contain approximately one cadmium atom per 6 cells above the stoichiometry or instead of doping ions Cr^{2+} or Cr^{3+}. However, the electrons from these cadmium ions do not enter the conduction band, since their concentration is 2 orders of magnitude higher than the concentration of electrons in a pure sample. The concentration of conduction electrons is $6 \cdot 10^{17}$ cm^{-3} in a pure sample. An excess (compared with similar regular positions of cadmium ions in the antifluorite lattice) spin density of s-electrons is observed on manganese ions in tetrahedral vacancies according to the ESR data [15] (which determines the electron Knight shift of g-factor of magnetic ion). It is possible that these nonstoichiometric cadmium ions or dopants in these positions are the sources of conduction electrons in the studied Dirac semimetal. The separation energies of the second electrons in cadmium and chromium atoms are very close, but the separation energy is lower for the third electron in chromium: 30.1 eV versus 37.5 eV for Cd [31]. The diameters of divalent chromium ions ($D_{Cr} \approx 1.66$ Å versus $D_{Cd} \approx 1.98$ Å and [31]) are significantly smaller than the substituted cadmium ions, and this leads to „subsidence“ of the lattice at the location of chromium doping ions and the occurrence of compression stresses in the nearest coordination spheres.

3.2. Electronic spin resonance

3.2.1. Evolution of the shape of the spectrum

Figure 1 shows a selection of field derivatives dP/dH of the ESR spectra at various temperatures. The upper part of the figure contains the spectra obtained at high temperatures, and the lower part contains the spectra obtained at low temperatures. The vertical dotted line

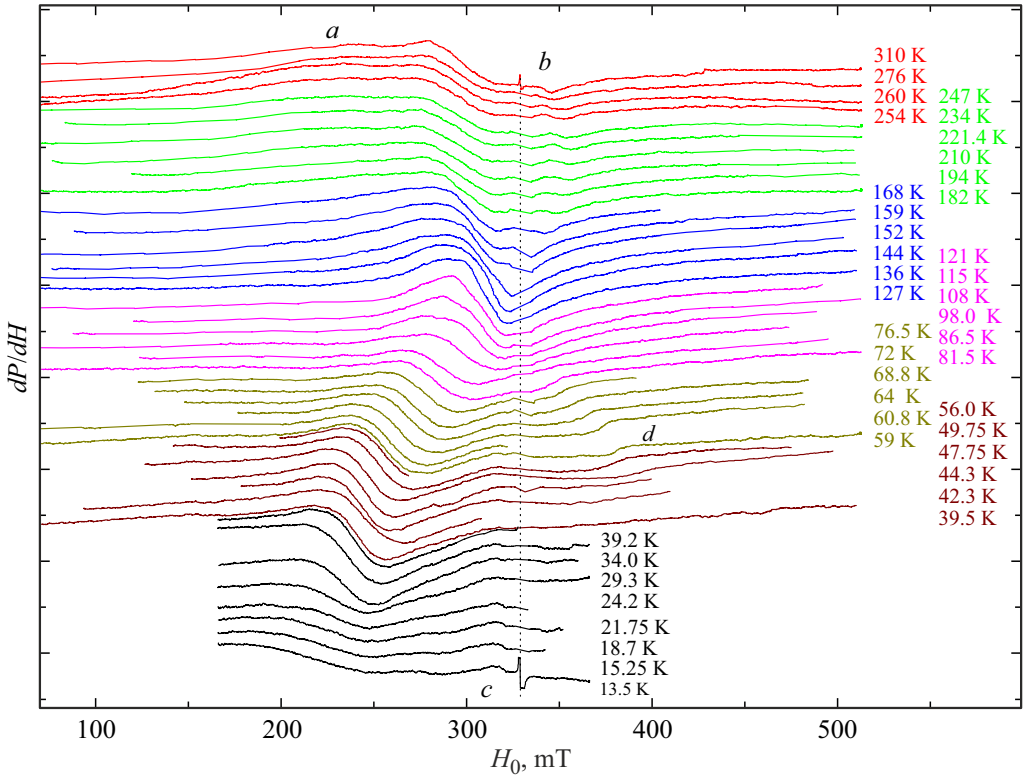

Figure 1. Variations of the ESR spectra of an oriented powder sample with temperature changes. The letters *a, b, c, d* denote the discussed features of the spectra, the behavior of the parameters of which are shown in other figures.

indicates the position of the diphenylpicrylhydrazyl (DPPH) reference signal. The signal itself is cut out of the spectra because it interferes with the perception of small features of the spectra by the eye. The temperatures related to the corresponding spectra are indicated on the right edge of the figure. We can conclude from the fact that the features of the spectrum obtained at a certain temperature are observed in the spectra obtained at close temperatures, that this feature really exists, and is not an accident caused by noise. Thus, we notice that the spectrum is a broad intense central line with a peak-to-peak width ΔH_{pp} of about 50 mT at high temperatures and significantly less intense lines with a width of about 15 mT located on its wings. It is clearly noticeable that the spectra are compressed with a decrease in temperature to 127 K, characterized by both a narrowing of the intense central line of the ESR spectrum and a shift to the center of weak satellites on its low-field and high-field wings. Only an intense central resonance line with the shape closest to the Lorentzian shape remains immediately below the temperature of 127 K. Referring to the temperature dependences of the resonant fields and the width of the centerline obtained from these spectra, shown in Figures 2 and 3, it can be seen that the entire spectrum narrows when the temperature drops to 127 K, which can only be interpreted as an exchange narrowing. A rapid shift of the main center line towards low fields takes place with a further decrease of temperature, indicating the transition of the entire impurity system to a ferromagnetic state. A sharp broadening of the main line of the ESR spectrum is observed with a further decrease of temperature, which is also characteristic of magnetic transitions. Moreover, a feature appears in the ESR spectrum (indicated in the figures by the letter *d*) when the main intense line shifts into low fields and this feature shifts into high fields relative to the point $H_0(T = 127\,\text{K})$ symmetrically to the shift of the main line into low fields. The feature *d* is an inverted ESR line. A weak signal, whose *g*-factor is close to parasitic signal of resonator $g \sim 2.06-2.08$ (from copper ions) but it has a smaller width, remains in the place of the shifted main line. It is possible that this signal has the same nature as weak ESR signals, indicated in the figure as *a* and *b*. Noting that the observed weak lines have approximately the same intensity, we have reason to attribute these lines to the lines of an hyperfine structure. The lines of the fine structure, as well as the lines traditionally derived from ions located in substitution positions and in tetrahedral vacancies, are obviously „hidden“ in the intense central line.

The natural content of ^{53}Cr isotope, from which the observed hyperfine structure obviously originates [32,33], is only 9.5%. However, the total intensity of the hyperfine structure lines in the experimental spectrum is estimated to be much lower. This is emphasized both by the smaller width of these lines (i. e., the concentration of ions from which the lines of the hyperfine structure originate

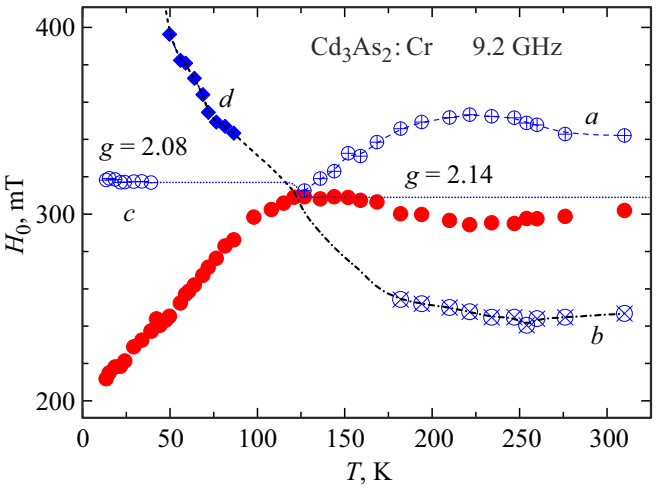

Figure 2. Temperature dependences of the position of the center line (full circles) and small features of the ESR spectrum of Cr^{3+} ions in α-Cd_3As_2. Features *a, b* — hyperfine structure lines (circles with crosses); feature *c* — mixture of a parasitic resonator signal from Cu^{2+} with a residual hyperfine ion structure line Cr^{3+} (empty circles); features of *d* — collapsed and inverted lines of the hyperfine structure of the ESR spectrum of $^{5}3Cr^{3+}$ ion (diamonds).

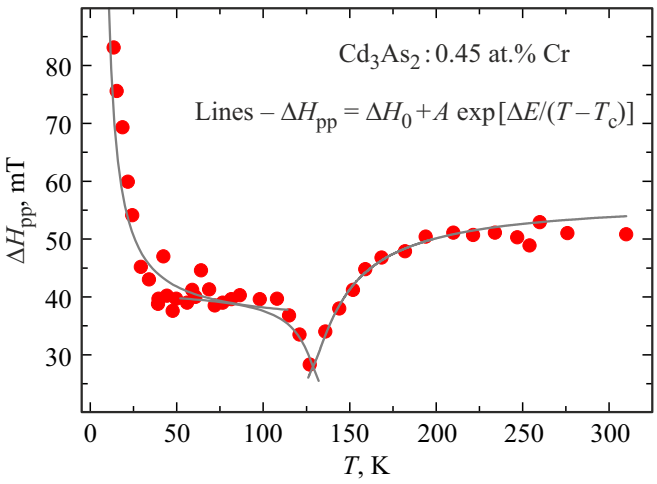

Figure 3. Temperature dependence of the peak width of the center line of the spectrum. The lines show dependencies of the form $\Delta H_{pp} = \Delta H_0 + A \cdot \exp[\Delta E/(T - T_c)]$. The dependency parameters for the temperature ranges of $T < 100$ K, $100\,\text{K} < T < 127$ K, $T > 127$ K are given in the text.

is significantly less than the expected value) and by the amplitude of the signal, and has the following explanation. Since the hyperfine structure is determined by the Fermi-contact interaction and is associated with the interaction of the magnetic moment of the nucleus with the spin density of electrons at the location of the nucleus, its manifestation is possible if ^{53}Cr nucleus has a spin density of *s*-electrons. We obtain an explanation for the low intensity of lines of an hyperfine structure considering that it was found in Ref. [15] for the case of manganese doping that the density of conduction *s*-electrons is observed only for tetrahedral vacancies (interstitial positions). Approximately 1/5 of the dopants fall into tetrahedral vacancies in the case of europium doping [34]. Assuming that the same ratio is maintained in the case of chromium doping, we obtain that the intensity of the hyperfine structure should be about 40 times less than the intensity of the central line. This corresponds to reality.

Let's consider the behavior of the ESR spectrum in the temperature range above 127 K. Figures 2 and 3 clearly show that the entire spectrum strongly narrows with a decrease of temperature. The maximum span of the hyperfine structure is 115 mT. Such an hyperfine spectrum structure collapses completely due to exchange narrowing at a temperature of about 127 K. The value of *g*-factor to which the ESR spectrum is clearly narrowed is $g = 2.14$. For comparison [20]: the anisotropic *g*-factor of Cr^{3+} ion has typical values $g_{\parallel} - g_{\perp} = 1.95-1.98$. The central line of the spectrum also strongly exponentially narrows by almost 2 times (see Figure 3). Establishing the fact of a complete narrowing of this line requires special studies on single crystal samples. However, this is most likely not happening for two reasons: 1) this narrowing takes place due to the strong exchange interaction of chromium ions through conduction *s*-electrons located in tetrahedral vacancies; 2) the majority of chromium impurity ions are in substitution positions and have a different character of exchange interaction. The range of interaction is ensured by the protection of the states of conduction electrons in a Dirac semimetal.

A strong narrowing of the resonant line can result in the saturation effect [20], since the relaxation of the microwave field energy absorbed during resonance becomes severely limited due to a critical increase of the magnetization relaxation time. This, in turn, can affect the shape of the resonance line according to Ref. [20,35–41], up to its collapse [39], and result in an inversion of its shape. Apparently, we observe this using the example of the feature *d*. Obviously, nonequilibrium magnetization should result in a change of the demagnetizing factor and a shift of the associated resonant signal.

3.2.2. Temperature dependences of the spectrum parameters

The temperature dependence of the line width $\delta H(T)$ can be determined by several mechanisms and corresponding contributions:

1) temperature-independent contribution;

2) linear Korringa contribution $\delta H(T) \propto T$;

3) fluctuation contribution (fluctuations of magnetization in the theory of Landau phase transitions give dependences of the type $\delta H(T) \propto (T - T)^{-1/2}$);

4) exchange broadening due to spin-spin exchange interactions in the presence of a gap ΔE separating the Fermi level from the filled zone, $\delta H(T) \propto \exp[\Delta E/T]$;

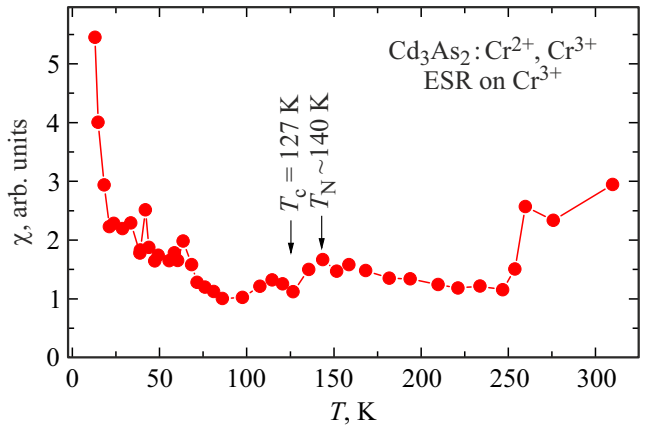

Figure 4. Temperature behavior of the intensity of the central line of the ESR spectrum. The data reflect only the nonmonotonic nature of the temperature behavior of the magnetic susceptibility of Cr^{3+} ions, since they are incorrect for a number of reasons: First of all, the center line is not a single line. Secondly, the line width decreases exponentially and may be associated with a decrease of the number of Cr^{3+} ions involved in the resonance. Therefore, the actual peak of paramagnetic susceptibility may not be at the point designated as the Neel temperature T_N, but at the point $T_c = 127$ K, defined for the minimum line width in Figure 3.

5) two-stage relaxation processes, and each stage can be controlled by its own mechanism with its own characteristic temperature $\delta H(T) \propto \exp[\Delta E/(T - T_c)]$;

6) exchange constriction $\delta H \sim (\delta H_0)^2/\delta H_{ex}$ (in original form [42–44] $\Delta\omega \propto (\Delta\omega_0)^2/\Delta\omega_{ex}$; $(\Delta\omega_0)^2$ or, in field units, $(\delta H_0)^2$ — square static dipole line width in the absence of exchange, and the exchange frequency $\Delta\omega_{ex}$ may increase with the decrease of temperature (and may be associated with the opening of a gap in the spectrum of electronic excitations, which blurs with the increase of the temperature).

The relaxation rate of the magnetic moment of an ion can be determined by the density of states at the Fermi level, which in turn can be modulated by changing the energy structure of the valence band and conduction band and filling their energy levels, for example, in the case of topological materials, due to the Landau level displacement.

The exchange narrowing of the spectrum takes place to a temperature of 127 K as can be seen from Figures 2 and 3. There is a weak maximum in the temperature dependence of the intensity of the main (central) signal (see Figure 4) at a temperature of about 140 K, which can be interpreted as evidence of the antiferromagnetic (AFM) transition. The temperature dependence of the resonant field also slightly increases in this temperature range (see Figure 2), which also supports the AFM transition. The width of the central resonance line rapidly decreases in this temperature range. This behavior is typical for AFM transitions. At the same time, a further rapid decrease of the resonant field indicates a ferromagnetic transition in a system with a low value of the demagnetizing factor, which, obviously, should have been set when the powder particles were oriented in a magnetic field.

As stated above, we observe a strong exchange narrowing of the spectrum, leading to the collapse of the hyperfine spectrum and saturation of the exchange-narrowed resonance line of the hyperfine structure. The effect of inversion of the shape of ESR line (see lines *d* in Figure 1 and their corresponding dependencies in Figure 2) indicated in Ref. [35–40] is a consequence of its saturation. The width of such an exchange-narrowed line is given by the ratio of the square of the dipole width to the exchange frequency. The width of the resonance lines will decrease exponentially if we assume that the frequency of exchange between Cr^{3+} ions through conduction electrons and Cr^{2+} ions exponentially increases as a result of condensation of exchange-coupled pairs of Cr^{2+}–Cr^{3+} ions into the AFM state. We used the expression $\Delta H_{pp} = \Delta H_0 + A \cdot \exp[\Delta E/(T - T_c)]$ to describe the temperature behavior of the width of the central resonance line of the spectrum. ΔH_0 means a temperature-independent contribution to the line width and a temperature-linear Korringa contribution in this expression. The temperature-independent contribution is estimated to be on the order of 38 mT, while the minimum width is 28 mT. The Korringa contribution is estimated from Figure 3 at no more than 0.053 mT/K.

The exponent describes the behavior of the width under the impact of two-stage relaxation processes associated with a change (increase or decrease) of the density of states near the Fermi level. The effective temperature is set in the denominator (by analogy with the Curie-Weiss law), which takes into account the exchange field through the characteristic ordering temperature T_c.

Solid lines in Figure 3 show three exponents $\Delta H_{pp} = \Delta H_0 + A \cdot \exp[\Delta E/(T - T_c)]$ that with a good quality describe the experimental data, differing in the following parameters:

at $T < 100$ K, $\Delta H_0 = 5.0$ mT, $A = 30$ mT, $\Delta E = 10$ K, $T_c = 1-5$ K;

at $100\,\text{K} < T < 127$ K, $\Delta H_0 = 26.5$ mT, $2A = 30$ mT, $\Delta E = 10$ K, $T_c = 133$ K;

at $T > 127$ K, ΔH_0=27.0 mT, A=30 mT, $-2\Delta E$=10 K, $T_c = 123$ K.

Since there is a divergence in this dependence for $T = T_c$, values close to but not equal to 127 K are taken as T_c: 133 and 123 K.

It should be noted that the observed dependencies can be described much better by „inverted“ exponents of type $\exp[(T - T_c)/\Delta E]$. However, such dependencies are not known and are not explained according to the data available in the literature. It should also be noted that the observed dependences are not related to a single line, but are related to the envelope of a set of resonant lines, which are both the result of the interaction of energy levels and the result of the superposition of lines on each other during measurement. This may also be the reason for discrepancies between experimental data and their mathematical description. The studies in Ref. [45,46] are of interest from the point of view

of the approaches used in the literature to the nature of the width of the magnetic resonance line.

The observed behavior of the resonant field and the line width can also be qualitatively described by inverse root temperature dependences of the type $\propto (T - T_c)^{-1/2}$, which follow from the theory of Landau phase transitions in the case of explanation of the observed dependences by fluctuations of magnetization. However, the behavior of the resonant field and the line width turn out to be related in this case, namely: the shift of the resonant field is equal to half the broadening of the resonant line. This is not observed in our experiment. Therefore, we associate the observed dependencies with processes caused by changes of the population of energy levels in case of two-stage electronic transitions. Therefore, the exponent uses a mathematical construction indicating the presence of an energy gap through which thermal excitation of electrons occurs near the Fermi level, and the characteristic temperature at which this energy gap is included.

4. Conclusion

Thus, we observe ESR on inclusions of Cr^{3+} ions located in the magnetic system of dopant ions Cr^{2+} and indicating the processes occurring in this system. Temperature dependences of resonant fields and line widths in the ESR spectra of this system (see Figures 2 and 3) indicate an increased exchange narrowing of the ESR spectrum and the presence of a magnetic phase transition near $T \approx 127$ K. A similar AFM transition was observed based on the temperature dependence of the static magnetic susceptibility in the system of magnetic impurities of divalent europium at close temperatures [34]. It should be emphasized that the value of g-factor is as abnormally high in the case of Cr^{3+} ions as in the case of europium ions. We associate this anomaly with the interaction of localized magnetic moments with conduction electrons having an extremely large g-factor in Cd_3As_2 matrix.

The experimentally detected inversion of the shape of the magnetic resonance line caused by the saturation in case of a sharp exchange narrowing (collapse) of the hyperfine structure of the ESR spectrum in a Dirac semimetal requires detailed study.

Funding

The work was carried out within the framework of the state assignment of the FRC Kazan Scientific Center of RAS No. EGISU 122011800133-2 (Yu.V. Goryunov) and the POLYOXYNANOMED Program, 011201 (A.N. Nateprov).

Conflict of interest

The authors declare that they have no conflict of interest.

References

[1] M.A. Ruderman, C. Kittel. Phys. Rev. **96**, *1*, 99 (1954).
[2] N. Bloembergen, T.J. Rowland. Phys. Rev. **97**, *6*, 1679 (1955).
[3] H.-R. Chang, J. Zhou, S.-X. Wang, W.-Y. Shan, D. Xiao. Phys. Rev. B **92**, *24*, 241103(R) (2015).
[4] E. Kogan. Phys. Rev. B **84**, *11*, 115119 (2011).
[5] E. Kogan, M. Kaveh. Physica Status Solidi B **252**, *12*, 2789 (2015). https://doi.org/10.1002/pssb.201552457
[6] J.-H. Sun, D.-H. Xu, F.-C. Zhang, Y. Zhou. Phys. Rev. B **92**, *19*, 195124 (2015).
[7] B.Q. Lv, T. Qian, H. Ding. Rev. Mod. Phys. **93**, *2*, 025002 (2021).
[8] D. Mastrogiuseppe, N. Sandler, S.E. Ulloa. Phys. Rev. B **93**, *9*, 094433 (2016).
[9] Y. Liu, R. Tiwari, A. Narayan, Z. Jin, X. Yuan, C. Zhang, F. Chen, L. Li, Z. Xia, S. Sanvito, P. Zhou, F. Xiu. Phys. Rev. B **97**, *8*, 085303 (2018).
[10] P. Villar Arribi, J.-X. Zhu, T. Schumann, S. Stemmer, A.A. Burkov, O. Heinonen. Phys. Rev. B **102**, *15*, 155141 (2020).
[11] M. Goyal, H. Kim, T. Schumann, L. Galletti, A.A. Burkov, S. Stemmer. Phys. Rev. Mater. **3**, *6*, 064204 (2019).
[12] M. Uchida, Y. Nakazawa, S. Nishihaya, K. Akiba, M. Kriener, Y. Kozuka, A. Miyake, Y. Taguchi, M. Tokunaga, N. Nagaosa, Y. Tokura, M. Kawasaki. Nature Commun. **8**, *1*, 2274 (2017). https://doi.org/10.1038/s41467-017-02423-1
[13] S.X. Zhang, J. Zhang, Y. Wu, T.T. Kang, N. Li, X.F. Qiu, P.P. Chen. Mater. Res. Express **7**, *10*, 106405(2020).
[14] Yu.V. Goryunov, A.N. Nateprov. Phys. Solid State **62**, *1*, 100 (2020).
[15] Yu.V. Goryunov, A.N. Nateprov. Phys. Solid State **63**, *2*, 223 (2021).
[16] G.S. Shakurov, A.G. Avanesov, S.A. Avanesov. Phys. Solid State **51**, *11*, 2292 (2009).
[17] D.A. Akhmetzyanov, V.B. Dudnikova, E.V. Zharikov, E.R. Zhiteitsev, O.N. Zaitseva, A.A. Konovalov, V.F. Tarasov. Phys. Solid State **55**, *3*, 520 (2013).
[18] P.B. Oliete, V.M. Orera, P.J. Alonso. Phys. Rev. B **53**, *6*, 3047 (1996).
[19] A.G. Avanesov, V.V. Badikov, G.S. Shakurov. Phys. Solid State **45**, *8*, 1451 (2003).
[20] S.A. Altshuler, B.M. Kozyrev. Elektronnyi paramagnitnyi rezonans soedineniy elementov promezhutochnykh grupp. Nauka, M. (1972). 672 p. Pp. 159–225. (in Russian).
[21] Yu.V. Goryunov, A.N. Nateprov. Phys. Solid State **65**, *3*, 361 (2023).
[22] N.Ya. Asadullina, M.M. Zaripov, V.A. Ulanov. FTT **39**, *2*, 302 (1997). (in Russian).
[23] J.J. Krebs, G.H. Stauss. Phys. Rev. B **15**, *1*, 17 (1977).
[24] M.N. Sarychev, N.Y. Ofitserova, I.V. Zhevstovskikh, A.V. Egorov, V.T. Surikov, N.S. Averkiev, V.V. Gudkov. ZhETF **165**, *2*, 226 (2024). (in Russian).
[25] M.G. Brik, N.M. Avram. J. Molecular Struct. **838**, *1–3*, 193 (2007).
[26] V.V. Bannikov, V.Ya. Mitrofanov. Phys. Solid State **47**, *8*, 1532 (2005).
[27] E.B. Olshanetsky, Z.D. Kvon, G.M. Gusev, N.N. Mikhailov, S.A. Dvoretsky, J.C. Portal. JETP Lett. **91**, *7*, 347 (2010).
[28] Y. Kumar, V.P.S. Awana. J. Supercond. Novel Magn. **34**, *5*, 1303 (2021). https://doi.org/10.1007/s10948-021-05910-1

[29] S. Borisenko, Q. Gibson, D. Evtushinsky, V. Zabolotnyy, B. Büchner, R.J. Cava. Phys. Rev. Lett. **113**, *2*, 027603 (2014). https://doi.org/10.1103/PhysRevLett.113.027603
[30] M.N. Ali, Q. Gibson, S. Jeon, B.B. Zhou, A. Yazdani, R.J. Cava. Inorg. Chem. **53**, *8*, 4062 (2014). https://dx.doi.org/10.1021/ic403163d
[31] A.I. Efimov, L.P. Belorukova, I.V. Vasilkova, V.P. Chechev, Svojstva neorganicheskih soedinenij. Spravochnik. Khimiya, L. (1983). 392 p. (in Russian).
[32] V.F. Tarasov, R.M. Eremina, K.B. Konov, R.F. Likerov, A.V. Shestakov, Yu.D. Zavartsev, S.A. Kutovoi. Appl. Magnetic Resonance **52**, *1*, 5 (2021). https://doi.org/10.1007/s00723-020-01225-x
[33] L.K. Aminov, I.N. Kurkin, B.Z. Malkin. Phys. Solid State **55**, *7*, 1343 (2013).
[34] Yu.V. Goryunov, A.N. Nateprov. Phys. Solid State **60**, *1*, 68 (2018).
[35] V.A. Atsarkin, S.K. Morshnev. JETP Lett. **6**, *4*, 88 (1967).
[36] V.A. Atsarkin. JETP **31**, *6*, 1012 (1970).
[37] V.F. Tarasov. JETP Lett. **68**, *5*, 394 (1998).
[38] K.M. Salikhov, V.F. Tarasov. Magn. Resonance Chem. **43**, S1, S221 (2005).
[39] R.T. Galeev. Phys. Solid State **48**, *5*, 871 (2006).
[40] K.M. Salikhov, I.T. Khairuzhdinov. JETP **128**, *5*, 684 (2019).
[41] K.M. Salikhov. Phys. — Uspekhi **62**, *10*, 951 (2019).
[42] C. Kittel. Introduction to Solid State Physics, 4th ed. John Wiley & Sons, Inc. New York, London, Sydney, Toronto (1971).
[43] J.H. Van Vleck. Phys. Rev. **74**, *9*, 1168 (1948).
[44] F. Keffer. Phys. Rev. **88**, *4*, 686 (1952).
[45] S.V. Gudenko, A.Yu. Yakubovskii, O.Yu. Gorbenko, A.R. Kaul. Phys. Solid State **46**, *11*, 2094 (2004).
[46] M.P. Trubitsyn. FTT **41**, *9*, 1668 (1999). (in Russian).

Translated by A.Akhtyamov